A Multi-Substrate Single-File Model for Ion-Coupled Transporters

Alyce Su,* Sela Mager,‡ Stephen L. Mayo,‡§ and Henry A. Lester‡
*Division of Physics, Mathematics and Astronomy, and ‡Division of Biology, §Howard Hughes Medical Institute, California Institute of Technology, Pasadena, California 91125 USA

ABSTRACT Ion-coupled transporters are simulated by a model that differs from contemporary alternating-access schemes. Beginning with concepts derived from multi-ion pores, the model assumes that substrates (both inorganic ions and small organic molecules) hop a) between the solutions and binding sites and b) between binding sites within a single-file pore. No two substrates can simultaneously occupy the same site. Rate constants for hopping can be increased both a) when substrates in two sites attract each other into a vacant site between them and b) when substrates in adjacent sites repel each other. Hopping rate constants for charged substrates are also modified by the membrane field. For a three-site model, simulated annealing yields parameters to fit steady-state measurements of flux coupling, transport-associated currents, and charge movements for the GABA transporter GAT1. The model then accounts for some GAT1 kinetic data as well. The model also yields parameters that describe the available data for the rat 5-HT transporter and for the rabbit Na^+-glucose transporter. The simulations show that coupled fluxes and other aspects of ion transport can be explained by a model that includes local substrate-substrate interactions but no explicit global conformational changes.

INTRODUCTION

Several classes of membrane transport proteins use electrochemical gradients for ions (usually Na^+ or H^+) to accumulate organic molecules (neurotransmitters, sugars, amino acids, osmolytes) in plant and animal cells (Schultz, 1986; Harvey and Slayman, 1994). The tight flux coupling between these inorganic and organic substrates constitutes a hallmark of ion-coupled transporters and contrasts with properties of ion channels, another major class of membrane transport proteins (Hille, 1992). To explain the mechanism of flux coupling, two major classes of model have been proposed (Hill, 1977; Schultz, 1980; Stein, 1986; Kanner and Schuldiner, 1987; Rudnick and Clark, 1993). Early models envisioned a recirculating carrier whose motions were largely governed by the binding and dissociation of the substrates. More recently, sequence analysis of cloned transporters suggests 6–12 putative transmembrane domains, rendering a recirculating carrier less plausible.

Most contemporary mechanistic concepts of ion-coupled transport employ the alternating-access scheme first enunciated by Jardetzky (1966) and developed in many papers by Laüger (see Laüger, 1979, 1991; Wright, 1993; Lester et al., 1994). In this scheme, ion-coupled transporters are viewed as pores or channels that have two gates. Whereas the pore has sites that bind, or perhaps merely accept, all of the permeant substrates, the gates have most of the (poorly understood) properties that ensure coupled transport. When all of the substrates are bound appropriately, the gates undergo conformational changes; and these conformational changes account for the differences in compartmentalization of the substrates during the transport cycle. Some alternating-access schemes incorporate ordered binding and dissociation of substrates (see, for instance, Rudnick and Clark, 1993). Now that cloned transporters can be expressed at high densities and studied with good temporal resolution in heterologous expression systems, additional measurements are available on pre-steady-state kinetics and charge movements associated with one or a few steps in the transport cycle (Parent et al., 1992a,b; Mager et al., 1993, 1994; Cammack et al., 1994; Wadiche et al., 1995a). Several studies build on these time-resolved data in the context of the alternating-access model (Parent et al., 1992b; Mager et al., 1993; Wadiche et al., 1995a).

However, the newer measurements have also revealed several additional classes of complexities that cannot be explained by straightforward alternating-access models: 1) There are leakage currents—Na^+ fluxes in the absence of organic substrate (Schwartz and Tachibana, 1990; Umbach et al., 1990; Cammack et al., 1994). 2) There are major departures from accepted stoichiometry, so that transport-associated currents are several times larger than the flux of organic substrate (Mager et al., 1994; Wadiche et al., 1995b; Galli et al., 1995; Picaud et al., 1995; Risso et al., 1995). 3) There are actual or inferred quantized current events that exceed by several orders of magnitude the single-charge events expected from the model (Mager et al., 1994; Wadiche et al., 1995b; DeFelice et al., 1995; Cammack and Schwartz, 1995).

Although more complex alternating-access models can be developed to account for some of these new phenomena, the time seemed ripe for an alternative class of models. Our formulation is termed the multi-substrate single-file transport model. We borrow heavily from ion channel models that incorporate a pore with several simultaneously bound ions (Hille, 1992). In particular, we do not explicitly allow conformational changes that change the compartmentalization of the

Received for publication 25 July 1995 and in final form 21 October 1995.
Address reprint requests to Dr. Henry A. Lester, Division of Biology 156-29, California Institute of Technology, Pasadena, CA 91125. Tel.: 818-395-4946; Fax: 818-564-8709; E-mail: lester@caltech.edu.

0006-3495/96/02/762/16 $2.00

substrates. The gates of the alternating-access model have been de-emphasized. Instead, functional compartmentalization arises because the pore (or lumen or channel) of the transporter mediates multiple substrate bindings and substrate-substrate interactions that favor, albeit only statistically, permeation in fixed ratios of inorganic ions to organic substrate.

In this first paper on the topic, we test the hypothesis of "multi-substrate single-file transport" in a quantitative, physically realistic fashion. We consider that the following three steady-state properties are most appropriate for detailed simulation: the ratio between the fluxes of organic and inorganic substrate, the electrical currents associated with the full transport cycle, and charge movements associated with partial steps of transport. We therefore simulate these properties of three ion-coupled transporters for which high-resolution functional studies have been reported: the GABA transporter GAT1 (Guastella et al., 1990; Mager et al., 1993), the serotonin transporter 5-HTT (Mager et al., 1994), and the Na^+-glucose transporter SGLT1 (Parent et al., 1992a,b). In each case, the multi-substrate single-file transport model has been found to reproduce available experimental data within experimental error (although charge movements have not been measured for 5-HTT). The model also accounts for newer phenomena such as leakage currents of all these transporters and variable stoichiometry of 5-HT transport, among other permeation properties.

Our approach has certainly been foreshadowed by many previous suggestions that transporters have channel-like mechanisms, for instance, in mediated ionic transport (Frohlich, 1988; Krupka, 1989; Dani and Levitt, 1990; Hasegawa et al., 1992), in electrogenic membrane systems (Andersen et al., 1985; Lagnado et al., 1988; Nakamoto et al., 1989; Hilgemann et al., 1991; Lauger, 1991; Wang et al., 1992; Gadsby et al., 1993; Rakowski, 1993), in neurotransmitter transporters (Krupka and Deves, 1988; Schwartz and Tachibana, 1990), and in facilitative sugar transporters (Barnett et al., 1975; Lowe and Walmsley, 1986; Kimmich and Randles, 1988; Walmsley, 1988; Baldwin, 1993; Hernandez and Fischbarg, 1994). Detailed theories have been based on electrodiffusion (Chen and Eisenberg, 1993; Eisenberg, 1994) and have treated channels that can simultaneously contain two ionic species at once (Franciolini and Nonner, 1994). Although molecular cloning has given us knowledge about the amino acid sequence of many ion-coupled transporters (Harvey and Nelson, 1994), there is still little relevant structural information at the atomic scale, or even at the level of tertiary structure or membrane topology or tertiary structure. Therefore the model is cast in purely formal terms at present.

THEORY AND METHODOLOGY

Structure of the model

The multi-substrate single-file transport model treats a transporter as a single file of binding sites, with ends open to the external and internal solutions (Fig. 1 *A*). The solutions are infinite sources and sinks: substrate concentrations within the solutions are not changed by the events of the simulation. Substrates are loaded from the solutions into the ion-coupled transporter lumen at rates governed partially by mass action. Once a substrate is within the ion-coupled transporter, it is allowed to move between sites and to the solutions. The kinetics of the ion-coupled transporter are reconstructed by combining all possible transitions.

Each of the N sites can be either empty or occupied by one of the m substrates. A total of N^{m+1} arrangements are possible. A state of the transporter is defined to be one such arrangement.

A hopping event is an allowed hop taken by a single substrate. Fig. 1 *B* shows the set of allowed hops. An allowed hop brings one substrate to an adjacent, empty site. Special rules apply to sites 1 and N (the external and internal solutions are considered to be adjacent to sites 1 and N, respectively). A substrate from the solution can hop onto site 1 or N only when the site is empty; however, a substrate on site 1 or N can always hop into the solution.

Hopping frequencies are rate constants that describe the probability of individual hopping events. Hopping frequencies $k_{a\to b}$ are described as the product $fg_v g_{ar}$. The first term f is called the "intrinsic hopping frequency" of a substrate; it is defined from mass action if the hop is from the solution and by a unimolecular event if the hop is from a binding site to another site within the membrane or to the solution. For

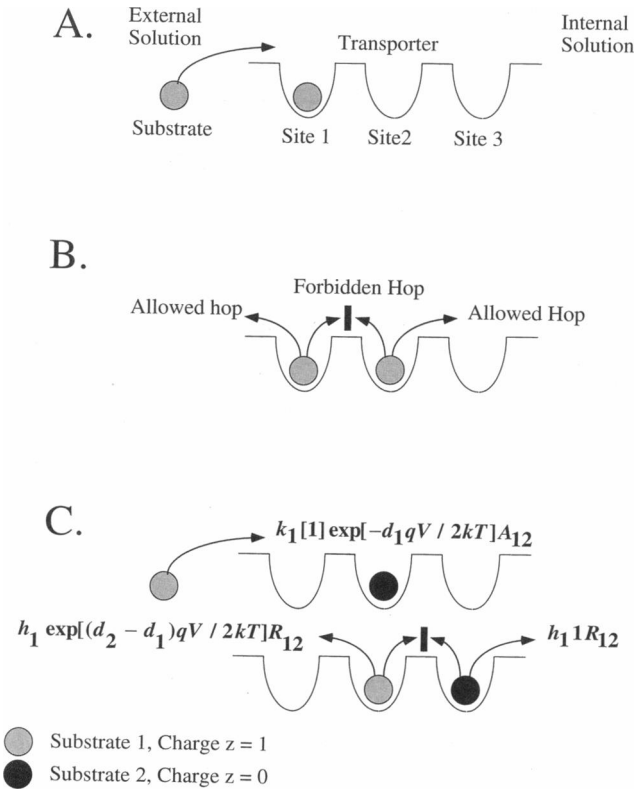

FIGURE 1 Multi-substrate single-file transport model. (*A*) Structure of the transporter, including three binding sites. The state, with a single bound substrate, corresponds to state 2 in Fig. 2. (*B*) Allowed hopping events. (*C*) Rules for obtaining the hopping frequencies, including the effects of voltage and of attraction/repulsion.

the present version of the model, the intrinsic hopping frequency varies with the substrate but is constant across all sites within the pore.

The second term, a dimensionless factor g_v, describes the effect of membrane potential on the intrinsic hopping frequency. The simple equations given below for the effect of potential are consistent with a model in which a) the membrane potential produces a linear field, b) there is a rate-limiting energetic barrier midway between each pair of sites, and c) the energy of the barrier with respect to each site is modified by the interaction between the charge on the substrate and the field.

The third term, a dimensionless factor g_{ar}, describes the effect of interactions with other substrates that occupy adjacent sites or, if an adjacent site is empty, the next site. g_{ar} is the product of an attraction term A and a repulsion term R. Examples are shown in Fig. 1 *C*. These attraction and repulsion terms also allow for the possibility that the field changes with the ionic contents of the channel.

For hops by a substrate i with charge zq in the presence of another substrate j (we include the possibility that $j = 0$ denotes an empty site)

$f = k_i[i]$ If it hops from the external solution to site 1, or from the internal solution to site N

$= h_i$ If it hops from a site within the transporter

$g_v = \exp[-(d_{s+1} - d_s)zq_iV/2kT]$ If it hops from site s to $s + 1$

$= \exp[(d_{s+1} - d_s)zq_iV/2kT]$ If it hops from site $s + 1$ to s

$g_{ar} = A_{ij}R_{ij;}$

A_{ij} Describes a hop that brings substrate i adjacent to substrate j

R_{ij} Describes a hop that separates substrate i from substrate j,

where

$[i]$ = concentration of substrate i in the solution

k_i = forward binding constant of substrate i in $M^{-1}\ s^{-1}$

h_i = intrinsic hopping frequency of substrate i in s^{-1}

d_s = fraction of electrical field sensed by a substrate with charge zq (s = 0 to $N + 1$, $d_0 = 0$, $d_{N+1} = 1$, $d_0 \le d_s \le d_{N+1}$)

V = membrane potential in mV

z = valence of a charged substrate

kT/q_i = ±25 mV, where
k = Boltzmann constant
T = Absolute temperature
q_i = Elementary charge on substrate i

A_{ij} = attractive coupling between two substrates separated by an empty site

R_{ij} = repulsive coupling between two substrates in adjacent sites

$A_{ij} = A_{ji}$, and $R_{ij} = R_{j,i}$, for i, j > 0; that is, the substrate-substrate couplings are symmetric

For each transporter configuration a, all transporter configurations b accessible from a by a single hopping event are linked. The corresponding hopping frequencies $k_{a\to b}$ are derived as described above. If configurations a and b cannot be linked by a single hopping event, then $k_{a\to b} = 0$. The final diagram is called a hopping diagram (Fig. 2), whose mathematical representation is a matrix $\boldsymbol{H}$ constructed as

$$H_{ab} = k_{b\to a} \tag{1}$$

$$H_{aa} = -\sum_{b=1,b\neq a}^{b=N^{m+1}} k_{a\to b}. \tag{2}$$

Given the hopping matrix $\boldsymbol{H}$, the time dependence of the ion-coupled transporter configuration distribution is

$$\frac{d\vec{x}}{dt} = \boldsymbol{H}\vec{x} \tag{3}$$

or equivalently,

$$\frac{dx_a}{dt} = \sum_{b=1}^{b=N^{m+1}} H_{ab}x_b = \sum_{b=1,b\neq a}^{b=N^{m+1}} H_{ab}x_b + H_{aa}x_a = \sum_{b=1,b\neq a}^{b=N^{m+1}} k_{b\to a}x_b - \sum_{b=1,b\neq a}^{b=N^{m+1}} k_{a\to b}x_a, \tag{4}$$

where $\vec{x} = (x_1, x_2, \ldots x_N{}^{m+1})$, $(0 \le x_a \le 1)$ represents the distribution of ion-coupled transporter configurations. For example, $x_1 = 0.25$ denotes that 25% of the transporters are in configuration 1.

At steady state, Eq. 4 reduces to

$$\frac{dx_a}{dt} = 0, \tag{5}$$

resulting in N^{m+1} linearly dependent homogeneous equations, of which $N^{m+1} - 1$ are linearly independent. The solution to Eq. 5 is a null space of dimension 1, which can be solved numerically by the Gauss-Jordan elimination method (Press et al., 1992). This solution yields predictions for several functional measurements, described in detail below.

A three-site two-substrate special case

For most of the simulations in this paper, we assume the following special case:

1. The transporter has $N = 3$ binding sites.

2. There are only $m = 2$ substrates, Na^+ (substrate 1) and the organic substrate (substrate 2). In particular, we disregard permeation by Cl^-. Our justification for this choice is a) that the role of Cl^- is rather less clear than that of the other substrates for most transporters (Mager et al., 1993; Lester et al., 1994) and b) that introducing another ion would complicate the simulations without adding much insight at this early stage.

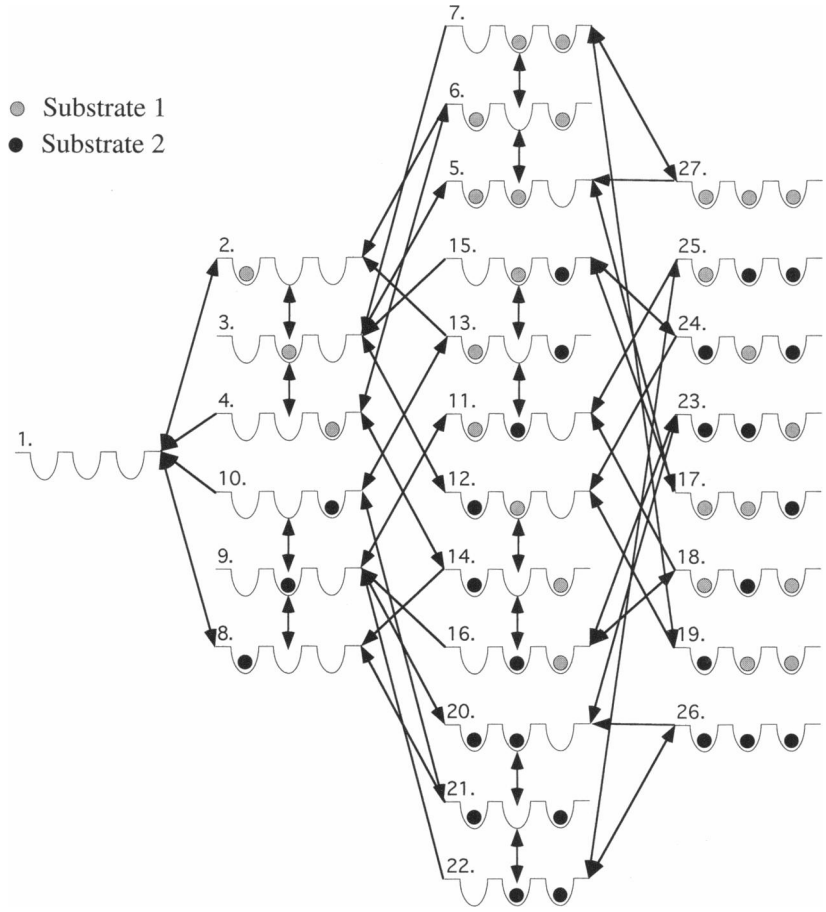

FIGURE 2 Hopping diagram for GAT1, 5-HT transporter, and SGLT1. This special case is used in most of our simulations. The ion-coupled transporter is modeled with three sites and two substrates, which generate a total of $3^{2+1} = 27$ transporter configurations. All transitions are reversible, except for those from the site 3 (rightmost) to the internal solution (an infinite sink).

3. The organic substrate has $q_2 = 0$ charge. This assumption holds for GABA and for the sugars but not for 5-HT$^+$ and is modified in some of the simulations described later.

4. The internal solution has zero concentration of all substrates. This assumption chiefly reflects the facts a) that oocyte experiments performed in our laboratory do not control intracellular concentrations and b) that these concentrations are thought to be small in most modern experiments. However, the assumption is modified in some simulations described below (for instance, data presented in Fig. 6).

The matrix elements corresponding to this special case are listed in Table 1 and the corresponding hopping diagram is shown in Fig. 2.

Steady-state predictions of the special case

Under these special conditions, Eq. 4 becomes

$$\frac{dx_a}{dt} = \sum_{b=1}^{27} H_{ab}x_b = \sum_{b=1,b\neq a}^{27} H_{ab}x_b + H_{aa}x_a = \sum_{b=1,b\neq a}^{27} k_{b\to a}x_b - \sum_{b=1,b\neq a}^{27} k_{a\to b}x_a, \tag{4a}$$

where $\vec{x} = (x_1, x_2, \ldots x_{27})$, $(0 \leq x_a \leq 1)$ represents the distribution of ion-coupled transporter configurations. Eq. 5 then becomes 27 linearly dependent homogeneous equations, of which 26 are linearly independent. The model makes predictions about three types of steady-state data.

Charge distribution

The simulated steady-state charge occupancy, $Q_\infty(V)$, is defined as follows:

$$Q_\infty(V) \equiv T\sum_{a=1}^{27} x_a Q_a = T\sum_{a=1}^{27} x_a \sum_{i=1}^{3} d_i q_i, \tag{6}$$

where T is the total number of transporters in the membrane and Q_a is the equivalent charge of the ath configuration. For instance, $Q_{26} = (d_1 + d_2 + d_3)q$ and $Q_{27} = 0$. We also define the maximum charge movement, from hyperpolarizing to depolarizing potentials, by $Q_{max} = Q(+\infty) - Q(-\infty)$.

Transport-associated current

The steady-state transport-associated current, I_∞, results from charged substrates moving fully across the membrane. This current is simulated by summing the charge movements that result from charged substrates hopping into the

TABLE 1 Hopping matrix elements for GAT1

	1	2	3	4	5	6	7	8	9	10	11	12	13	14	15	16	17	18	19	20	21	22	23	24	25	26	27
1		R01 h1 exp[d1 (v/50)]		R01 h1 exp[-(1-d3)(v/50)]				R02 h2		A02 h2																	
2	A01 P1		R01 h1 exp[(d2-d1)(v/50)]			R01 h1 exp[-(1-d3)(v/50)]							R02 h2														
3		A01 h1 exp[-(d2-d1)(v/50)]		A01 h1 exp[d2-d1)(v/50)]	R11 h1 exp[d1 (v/50)]		R11 h1 exp[-(1-d3)(v/50)]								R12 h2												
4			R01 h1 exp[-(d3-d2)(v/50)]			R01 h1 exp[d1 (v/50)]								R02 h2			R12 h2										
5			A11 P1			R11 h1 exp[(d3-d2)(v/50)]																						R11 h1 exp[-(1-d3)(v/50)]
6				A01 P1	R11 h1 exp[-(d3-d2)(v/50)]		R11 h1 exp[-(d2-d1)(v/50)]																					
7						A11 h1 exp[(d2-d1)(v/50)]													R12 h2									R11 h1 exp[d1(v/50)]
8	A01 P2								R02 h2					R01 h1 exp[-(1-d3)(v/50)]							R02 h2						
9								A01 h2		A02 h1	R12 h1 exp[d1(v/50)]					R12 h2 exp[-(1-d3)(v/50)]				R22 h2		R22 h2					
10									R02 h2				R01 h1 exp[d1(v/50)]								R02 h2						
11									A12 P1				A12 h2												R22 h2		
12			A12 P2											A12 h1										R12 h2			
13										A01 P1	R12 h2	R12 h2															
14				A01 P2								R12 h1 exp[-(d2-d1)(v/50)]															
15													A01 h1 exp[-(d2-d1)(v/50)]											R12 h2			
16		R12 h2												A12 h2									R22 h2				
17	A11 P1																										
18		A12 P1																									
19							A12 P2																			R22 h2	
20									A22 P2												A22 h2		R12 h2 exp[-(1-d3)(V/50)]				
21										A02 P2												R22 h2					
22																				A22 h2					R12 h2		
23		A22 P2																									
24	A12 P2																										
25																						A12 P1					
26																						A22 P2					
27							A11 P1																				

The matrix elements corresponding to the special case given in the text; the corresponding hopping diagram is shown in Fig. 2. H_{ba} corresponds to a hopping event from configuration a to configuration b. For example, the matrix element H_{21} is the same as $k_{1\to2}$. Each diagonal element is the negative of the sum of all the entries in the same column. For GAT1, substrate 1 is Na^+ and substrate 2 is GABA. P1 = $k_1[Na^+]\exp(d_1V/50)$. P2 = $k_{21}[GABA^+]$.

internal solution, e.g., $k_{27\to5}$. For our special case in which Na^+ is the only charged substrate, the steady-state transport-associated current is

$$I_\infty \equiv Tq[(x_4k_{4\to1}) + (x_6k_{6\to2}) + (x_7k_{7\to3}) + (x_{14}k_{14\to8}) + (x_{16}k_{16\to9}) + (x_{18}k_{18\to11}) + (x_{19}k_{19\to12}) + (x_{23}k_{23\to20}) + (x_{27}k_{27\to5})]. \quad (7)$$

Flux ratios

Steady-state flux coupling between substrates i and j is summarized by the ratio between the fluxes of i and j ($flux_i/flux_j$). The flux ratio between Na^+ and the organic substrate is

$$\frac{flux_1}{flux_2} \equiv \frac{[(x_4k_{4\to1}) + (x_6k_{6\to2}) + (x_7k_{7\to3}) + (x_{14}k_{14\to8}) + (x_{16}k_{16\to9}) + (x_{18}k_{18\to11}) + (x_{19}k_{19\to12}) + (x_{23}k_{23\to20}) + (x_{27}k_{27\to5})]}{[(x_{10}k_{10\to1}) + (x_{13}k_{13\to2}) + (x_{15}k_{15\to3}) + (x_{17}k_{17\to5}) + (x_{21}k_{21\to8}) + (x_{22}k_{22\to9}) + (x_{24}k_{24\to12}) + (x_{25}k_{25\to11}) + (x_{26}k_{26\to20})]}. \quad (8)$$

Available experimental data

The predictions described above were compared with the appropriate experimental data using algorithms described in the next section. Our most complete experimental data are available for GAT1. For instance, the experimental data on steady-state charge distribution was measured from voltage jumps in the absence of GABA (Mager et al., 1993). The integration of the transient response gives the total number of charges within the membrane. For purposes of these calculations, we abstracted the data of Mager et al. (1993) into the following functional form, which describes the data:

$$Q_\infty(V) = \frac{Nq}{1 + e^{-(V-V_h)/28.1}}. \quad (9)$$

A time interval of 0.2 ms was adequate for the simulations because the steady-state $\bar{x}$ obtained by integration and the Gauss-Jordan elimination method deviated by less than 0.001%. The steady-state transport-associated currents I_∞ were also taken from the data of Mager et al. (1993). The flux ratios $flux_1/flux_2$ for Na^+/GABA were assumed to lie between 1 and 2 (Kanner and Schuldiner, 1987).

Parameter searches

A set of randomly selected parameter values was used to start a simulation (Fig. 3). Gauss-Jordan elimination (Press et al., 1992) was used to solve Eq. 5 for the 27 x_a values. These values in turn yielded the three steady-state

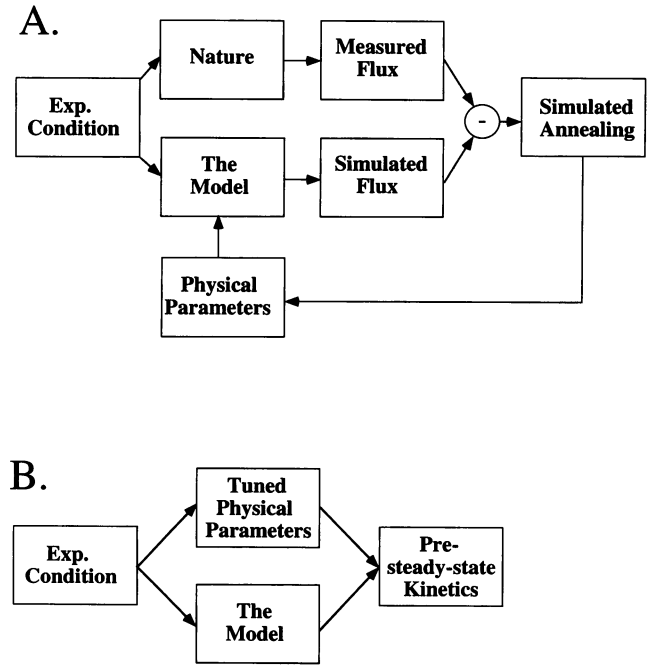

FIGURE 3 Simulation scheme. (*A*) Fitting mode. Simulated annealing is employed to optimize the parameter values by minimizing the error between the experimental and the simulated steady-state data. The resulting values are then used to predict the pre-steady-state kinetics. (*B*) Predicting mode. The resulting values from *A* are then used to predict transient currents.

predictions above: charge distribution, steady-state current, and flux ratio. Simulated annealing (Ingber, 1993) was employed to optimize the parameter values by minimizing the error between the experimental and the simulated steady-state data. The simulated annealing algorithm written in c was obtained by FTP from http://www.alumni.caltech.edu/~ingber/. Convergence was specified by an annealing temperature of 10^{-7} (Ingber, 1993). Fitting sessions required ~8 h on a Silicon Graphics Challenge workstation with 200-MHz R4400 processors.

Finally, we note that the exemplar physiological experiments in the paper by Mager et al. (1993) were performed on distinct oocytes, each expressing an unknown number of transporters. To calculate the total number of transporters T expressed in these exemplar oocytes from the Q_{max} data for each oocyte, we would have to assume values for d_1, d_2, and d_3. Therefore the flux per transporter was not accessible from the procedures presented thus far; and the hopping rate constants were uncertain by a common multiplicative constant. We could, however, make use of the experimentally determined value, $I_\infty/Q_{max} = 5.3\ s^{-1}$, where I_∞ is measured at 96 mM Na^+, 0.1 mM GABA, and −80 mV (Mager et al., 1993). This additional constraint in the simulations allowed us to determine the absolute values of the rate constants. The calculations are presented for $T = 1.18 \times 10^{11}$ transporters per cell (presumably a *Xenopus* oocyte expressing GAT1).

Calculation of transient currents

Simulated transient data for GAT1 were not used in the parameter search algorithm; instead, they were used as independent tests of our theories and parameters after the simulated annealing yielded several sets of parameters with nearly equal cost function values for the steady-state data. Transients were simulated by numerical integration, using Mathematica. The transient currents are given by the sum of all hopping events involving the movement of charge into or within the membrane weighted by the electrical distance traveled. Voltage jump relaxations for GAT1 were simulated using the experimental protocol; that is, for fixed $[Na^+]$ and zero GABA, the membrane potential was stepped between values as shown in Fig. 5. The voltage jump transients for GAT1 are defined as

$$\frac{I(t)}{Tq} \equiv d_1\left\{\begin{array}{l}[(x_1k_{1\to2}) - (x_2k_{2\to1})] + [(x_3k_{3\to5}) - (x_5k_{5\to3})] \\ + [(x_4k_{4\to6}) - (x_6k_{6\to4})] + [(x_9k_{9\to11}) - (x_{11}k_{11\to9})] \\ + [(x_{10}k_{10\to13}) - (x_{13}k_{13\to10})] + [(x_{15}k_{15\to17}) - (x_{17}k_{17\to15})] \\ + [(x_{16}k_{16\to18}) - (x_{18}k_{18\to16})] + [(x_7k_{7\to27}) - (x_{27}k_{27\to7})] \\ + [(x_{22}k_{22\to25}) - (x_{25}k_{25\to22})]\end{array}\right\}$$

$$+ (d_2 - d_1)\left\{\begin{array}{l}[(x_2k_{2\to3}) - (x_3k_{3\to2})] + [(x_6k_{6\to7}) - (x_7k_{7\to6})] \\ + [(x_{13}k_{13\to15}) - (x_{15}k_{15\to13})]\end{array}\right\} \quad (10)$$

$$+ (d_3 - d_2)\left\{\begin{array}{l}[(x_3k_{3\to4}) - (x_4k_{4\to3})] + [(x_5k_{5\to6}) - (x_6k_{6\to5})] \\ + [(x_{12}k_{12\to14}) - (x_{14}k_{14\to12})]\end{array}\right\}$$

$$+ (1 - d_3)$$

$$\times\left\{\begin{array}{l}[(x_4k_{4\to1}) + (x_6k_{6\to2})] + [(x_7k_{7\to3}) + (x_{14}k_{14\to8})] \\ + [(x_{16}k_{16\to9}) + (x_{18}k_{18\to11})] + [(x_{19}k_{19\to12}) + (x_{23}k_{23\to20})] \\ + [(x_{27}k_{27\to5})]\end{array}\right\},$$

where all x values are time dependent. Concentration-jump relaxations were simulated by stepping one or two substrate concentrations while holding other parameters fixed. For simplicity, relaxation kinetics were characterized by fitting to a single exponential component.

RESULTS

Figs. 4, 5, 6, 7, and 8 show the simulation results for the ion-coupled transporters GAT1, 5-HTT, and SGLT1. Optimized parameter values are listed in Table 2.

Simulation of GAT1 function

We devoted most effort to simulating GAT1 function, because we have access to extensive data for this ion-coupled transporter. GAT1 is a neurotransmitter transporter belonging to the plasma membrane Na^+/Cl^- coupled subfamily (Amara and Arriza, 1993). It drives the neurotransmitter GABA up its concentration gradient by cotransporting Na^+ down its electrochemical potential gradient (Keynan and Kanner, 1988). Electrophysiological data, tracer flux measurements, and thermodynamic measurements all suggest that 2 Na^+ ions are transported along with a single GABA molecule (Lester et al., 1994); and we have therefore used a special case of our model that includes three binding sites, so that these three molecules may bind simultaneously. Cl^- is another possible substrate for GAT1, but its role is not clear at the moment (Lester et al., 1994); therefore we felt it inappropriate at present to complicate the simulations by including Cl^-.

The experimentally determined permeation properties of GAT1 include steady-state currents as a function of Na^+ and GABA, leakage currents (Na^+ flux in the absence of GABA), substrate flux ratio, charge distribution, and gating currents induced by voltage jumps (Mager et al., 1993; Cammack et al., 1994). We note that leakage currents were not reported in our study of GAT1 function (Mager et al., 1993) but were reported by Cammack et al. (1994). In unpublished recent work, we have indeed found small inward currents that are suppressed by GABA uptake inhibitors in the absence of GABA itself; although we lack systematic data, these leakage currents are <5% of the maximal GABA-induced currents.

The model accounts well for the data that we used to fit the parameters, as summarized in Fig. 4. Five sets of parameters, each resulting from a simulated annealing run, had nearly equal cost function values and provided similar simulations of these data; the simulations of Fig. 4 were calculated with the parameters that also provided good simulations of transient currents (these parameters are given in Table 2). GAT1 steady-state currents are shown as a function of $[Na^+]$ in Fig. 4 *A*; note that the simulation dose-response relations show the observed sigmoidal dependence on $[Na^+]$. The simulations also show the expected hyperbolic dependence on [GABA] in Fig. 4 *B*. The simulations showed leakage currents of ~1% of the saturation current in the absence of external GABA (Fig. 4 *C*). A Na^+/GABA flux ratio between 1 and 2 was obtained (Fig. 4 *D*); the simulated flux ratio depends on membrane potential, a point that has not been tested experimentally for GAT1. The steady-state charge distribution exhibited a sigmoidal dependence on membrane voltage, and the midpoint was shifted to more negative voltages with decreasing $[Na^+]$; these features agree quantitatively with the experimental data (Fig. 4 *E*).

Transient currents

As a further qualitative test of the model, parameter sets from the simulated annealing were tested for their ability to simulate various transient currents. One parameter set survived this test; Fig. 5 displays some results. The simulated voltage-jump relaxations in the absence of GABA, shown in Fig. 5 *A*, display the general features described by Mager et al. (1993) and Cammack et al. (1994): for hyperpolarizing jumps, the transients are negative and consist of a rapid

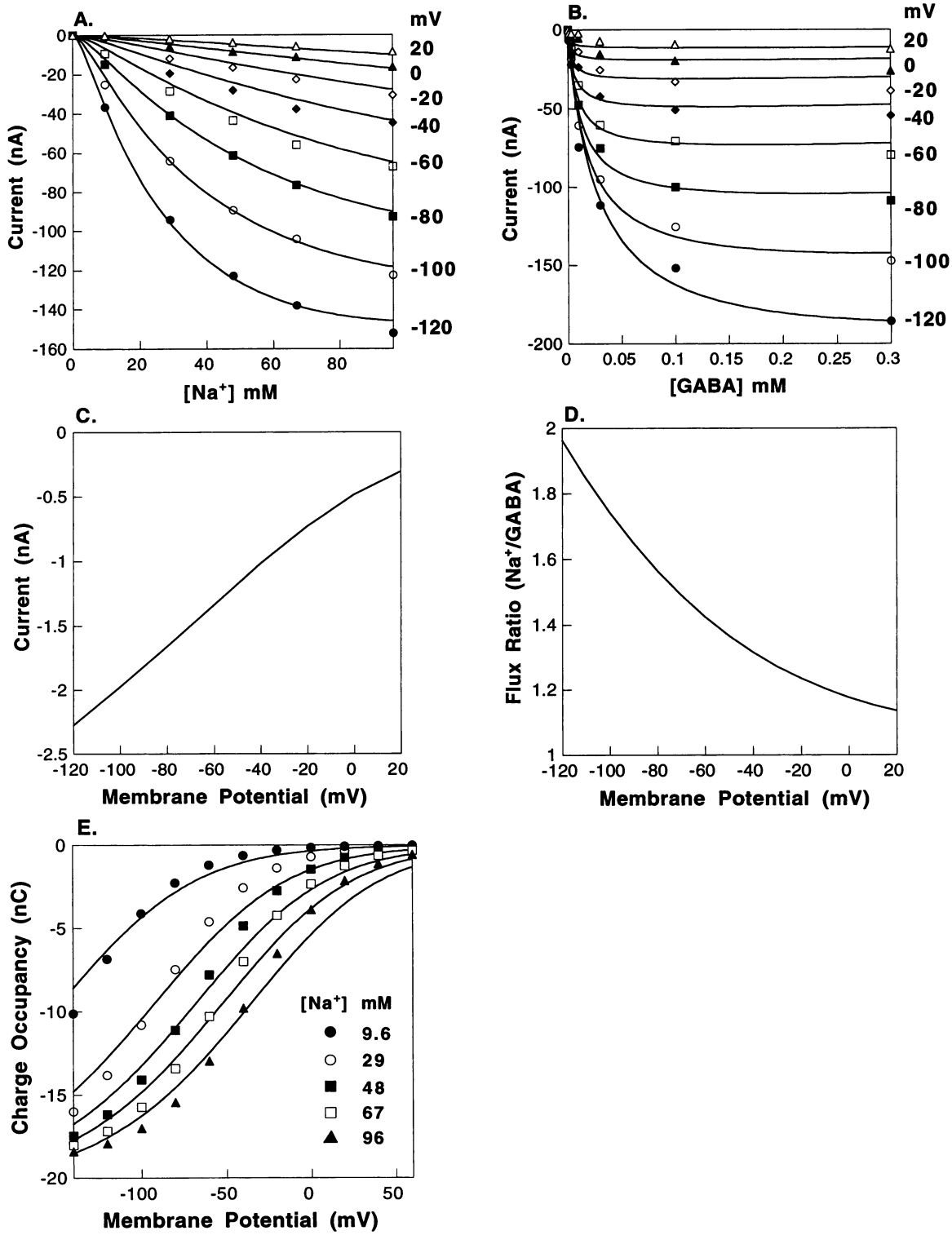

FIGURE 4 Simulated versus experimental GAT1 steady-state properties. Smooth lines are the simulations, using the parameters in Table 2. (*A*) Steady-state current as a function of $[Na^+]$. Experimental data from Mager et al. (1993). [GABA] = 0.1 mM, membrane potentials as indicated. (*B*) Steady-state current as a function of [GABA]. Experimental data from Mager et al. (1993). $[Na^+]$ = 96 mM; membrane potentials as in *A*. (*C*) Simulated leakage current at zero [GABA] versus voltage. (*D*) Flux ratio of Na^+ to GABA simulated at $[Na^+]$ = 96 mM, [GABA] = 0.3 μM, for the voltage range from −120 to 20 mV. (*E*) Steady-state charge distribution as a function of membrane potential in the absence of GABA. Experimental data from Mager et al. (1993), represented by Eq. 9. The curves are parametric in $[Na^+]$ as indicated.

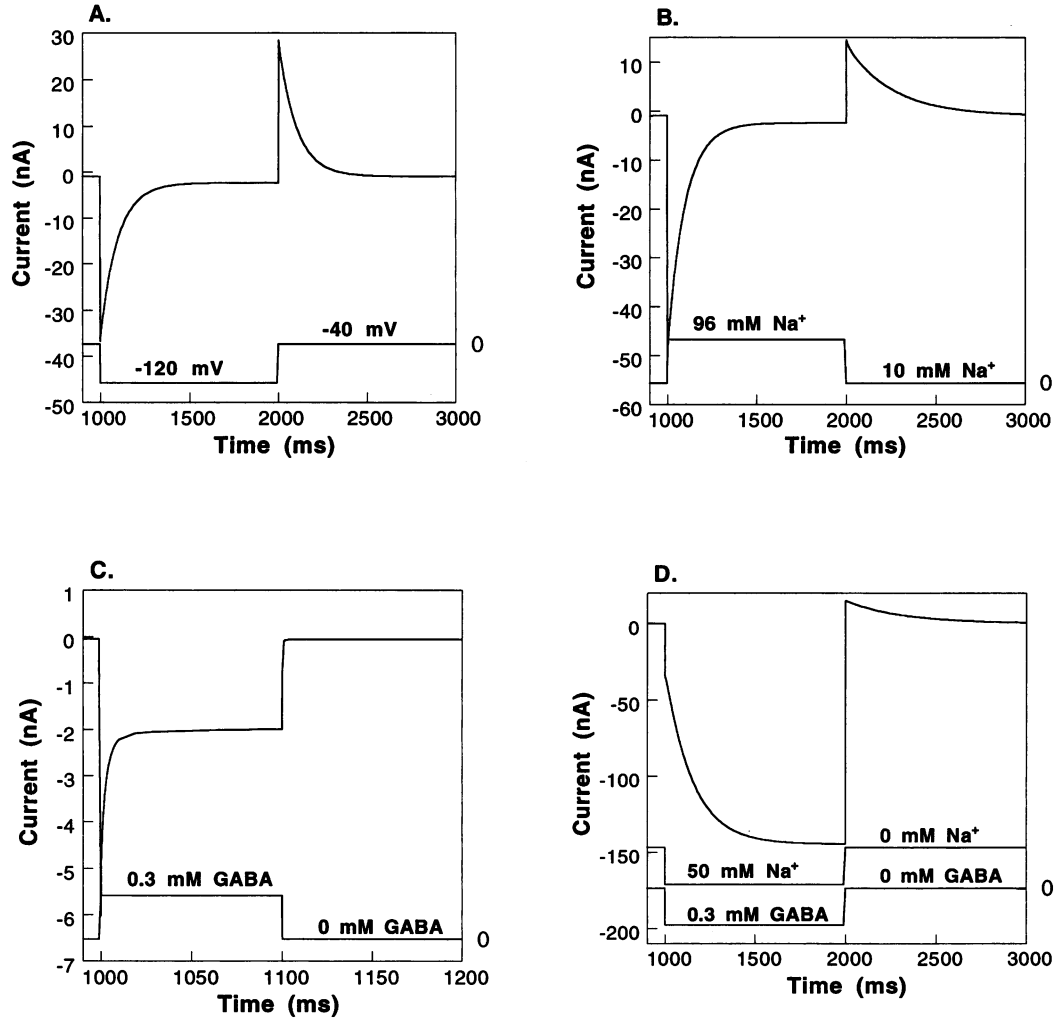

FIGURE 5 Simulated GAT1 transient currents. (*A*) Transient current for voltage jumps in the absence of GABA, at $[Na^+]$ = 96 mM. The membrane potential was held at −40 mV, stepped to −120 mV at time = 1 s, and stepped back to −40 mV at time = 2 s. (*B*) Transient current during $[Na^+]$ jumps in the absence of GABA, with membrane voltage clamped at −120 mV. $[Na^+]$ was held at 10 mM, stepped to 96 mM at time = 1 s, and stepped back to 10 mM at time = 2 s. (*C*) Transient current during [GABA] jumps, with $[Na^+]$ = 10 mM and membrane voltage clamped at −10 mV. [GABA] was held at 0 mM, stepped to 0.3 mM at time = 1 s, and stepped back to 0 mM at time = 1.1 s. (*D*) Transient current during simultaneous $[Na^+]$ and [GABA] jumps, with voltage clamped at −120 mV. $[Na^+]$ was held at 0 mM, stepped to 50 mM at time = 1 s, and stepped back to 0 mM at time = 2 s. [GABA] was held at 0 mM, stepped to 0.3 mM at time = 1 s, and stepped back to 0 mM at time = 2 s.

rising phase followed by a decay over several hundred milliseconds. For depolarizing jumps, the direction of the transient is reversed. The integral of these relaxations is represented by the steady-state charge distributions (Fig. 4 *E*); and we have verified that these simulated charge movements are equal and opposite for the jumps in both directions between a pair of potentials (Mager et al., 1993). The simulated relaxation time constant lies in the range of 70–150 ms and displays a maximum at negative membrane potentials (not shown), in agreement with experimental data (Mager et al., 1993; Cammack et al., 1994; S. Mager, preliminary unpublished results).

Simulated $[Na^+]$ and [GABA] jump-induced transients are shown in Fig. 5, *B* and *C*, respectively; and Fig. 5 *D* shows simulated simultaneous jumps of both substrate concentrations. There are no published data available for comparison with Fig. 5 *B*. The waveforms in Fig. 5, *C* and *D*, however, reproduce the general features observed by Cammack et al. (1994). Thus, the simulated jump from 0 to 0.3 mM GABA produces a transient peak on the millisecond time scale, followed by a sustained transport-associated current (Fig. 5 *C*) and compares well with figure 9 of Cammack et al. (1994). Furthermore, the simulated jump to 50 mM Na^+ and 0.3 mM GABA produces a rapid rise followed by a slower rise on the time scale of several hundred milliseconds, in agreement with figure 9 of Cammack et al. (1994). The simulated relaxations are more rapid than the published records for the jump back to 0 [GABA] and 0 $[Na^+]$, and there is a small simulated outward charge movement in Fig. 5 *D*; but these discrepancies could arise if the experimental solution changes are slightly slower than expected.

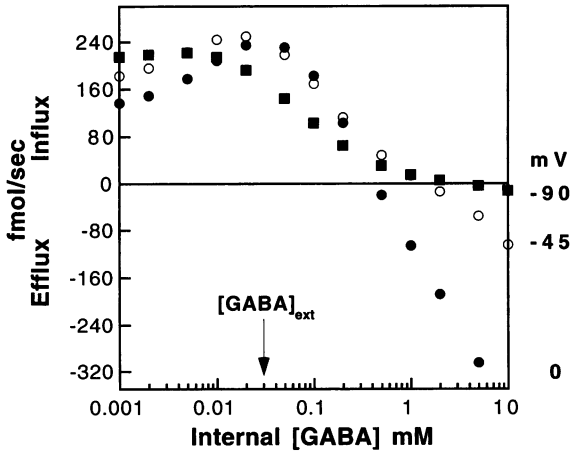

FIGURE 6 GAT1 transport up a concentration gradient. Simulation of Na^+-coupled GABA transport against a GABA concentration gradient. The external and internal [Na^+] were set to 96 and 5 mM, respectively. The external [GABA] was set to 0.03 mM, and the internal [GABA] was varied. GABA fluxes were simulated for membrane potentials of 0 mV, −45 mV, and −90 mV. Thus the electrochemical gradient for Na^+ alone favors Na^+ influx. Net GABA *influx* still occurs despite the fact that the [GABA] gradient alone favors GABA *efflux*.

Transport against a [GABA] gradient

In all of the simulations above, the internal concentrations of substrates are assumed to be zero. We relaxed this assumption to demonstrate the most important functional role of ion-coupled cotransporters: they drive the organic substrate up its concentration gradient by using the electrochemical potential gradient of an ionic substrate. For simplicity—and in the absence of real data on this point—we assumed that the forward binding constants k_i are the same for the internal and external sides of the membrane. The external and internal [Na^+], and membrane potential are adjusted to drive the Na^+ flow inward. The internal [GABA] was set higher than the external [GABA]; therefore net GABA efflux would occur if GABA cannot couple to the electrochemical potential gradient of Na^+. However, the simulation results in a net GABA influx (Fig. 6), suggesting that the multi-substrate single-file transport model does support transport up the chemical gradient of the organic substrate.

The attraction and repulsion terms

In the multi-substrate single-file transport model, the physical meanings of k_i, h_i, and d_s are transparent and represent common concepts in membrane transport. We comment here on the physical meaning of the attraction and repulsion parameters, A_{ij} and R_{ij}, respectively. Consider, for example, A_{12} and R_{12}, and focus on the transitions between transporter configurations 14 and 16.

$$k_{14\to16} = A_{12}h_2 \tag{11}$$

$$k_{16\to14} = R_{12}h_2 \tag{12}$$

We can define an equilibrium "association constant" for the state in which substrate 2 (GABA) is adjacent to substrate 1 (Na^+):

$$K_{12} = \frac{k_{16\to14}}{k_{16\to14}} = \frac{A_{12}}{R_{12}} = K_o \exp(-\Delta G_{12}/kT) \tag{13}$$

where K_o is a constant standard state factor involving the translational partition function of the ion (McQuarrie, 1976), k is the Boltzmann constant, T is the absolute temperature, and ΔG_{12} is the relative free energy between any pair of states, such as 14 and 16, in which these two substrates move adjacent to each other. If there are no couplings between substrates 1 and 2, then we expect no difference in the relative free energy, which will lead to a ratio of $A_{12}/R_{12} = 1$. However, if A_{12}/R_{12} is not equal to 1, the two substrates are said to be coupled. For instance, if the optimized values of A_{12} and R_{12} are such that $A_{12}/R_{12} > 1$, moving the two substrates together is favored. By more classical arguments, the ratio of k_i $[i]/h_i$ controls the energetics of moving substrate i into the ion-coupled transporter. Generalizing this argument to attractive and repulsive couplings between substrates, we obtain the following rules for GAT1:

1. Moving Na^+ into the transporter is favored at high [Na^+].
2. Moving GABA into the transporter is favored at high [GABA].
3. Moving Na^+ and GABA adjacent to each other is favored.
4. Moving Na^+ and Na^+ adjacent to each other is favored. This is the most surprising result of our analysis.
5. Moving GABA and GABA adjacent to each other is not favored.

According to these microscopic rules, at high [Na^+] and [GABA], we expect transporter configurations with more than two GABA molecules to be underpopulated. This is indeed the case. Under such conditions, the simulated population of transporter configurations 20, 21, 22, 23, 25, and 26 is negligible (Fig. 2). This may be due to the favored adjacencies between Na^+ and GABA (Rule 3).

Simulation of 5-HT transporter function

5-HTT is another ion-coupled neurotransmitter transporter belonging to the plasma membrane Na^+/Cl^--coupled family. It is known to accumulate 5-HT^+ in the presence of Na^+, Cl^-, and K^+. Na^+ and K^+ are cotransported and countertransported with 5-HT^+, respectively. The argument that Cl^- is cotransported with 5-HT^+ is somewhat less direct, as it has been difficult to demonstrate 5-HT^+ accumulation with only the Cl^- gradient as a driving force. The K^+ is coupled to the 5-HT^+ accumulation but is not required, for the transport still occurs in the absence of K^+ (Rudnick and Clark, 1993). Therefore, only Na^+ and 5-HT^+ are included in our model. Our 5-HT transporter model, like our GAT1 model, has three binding sites.

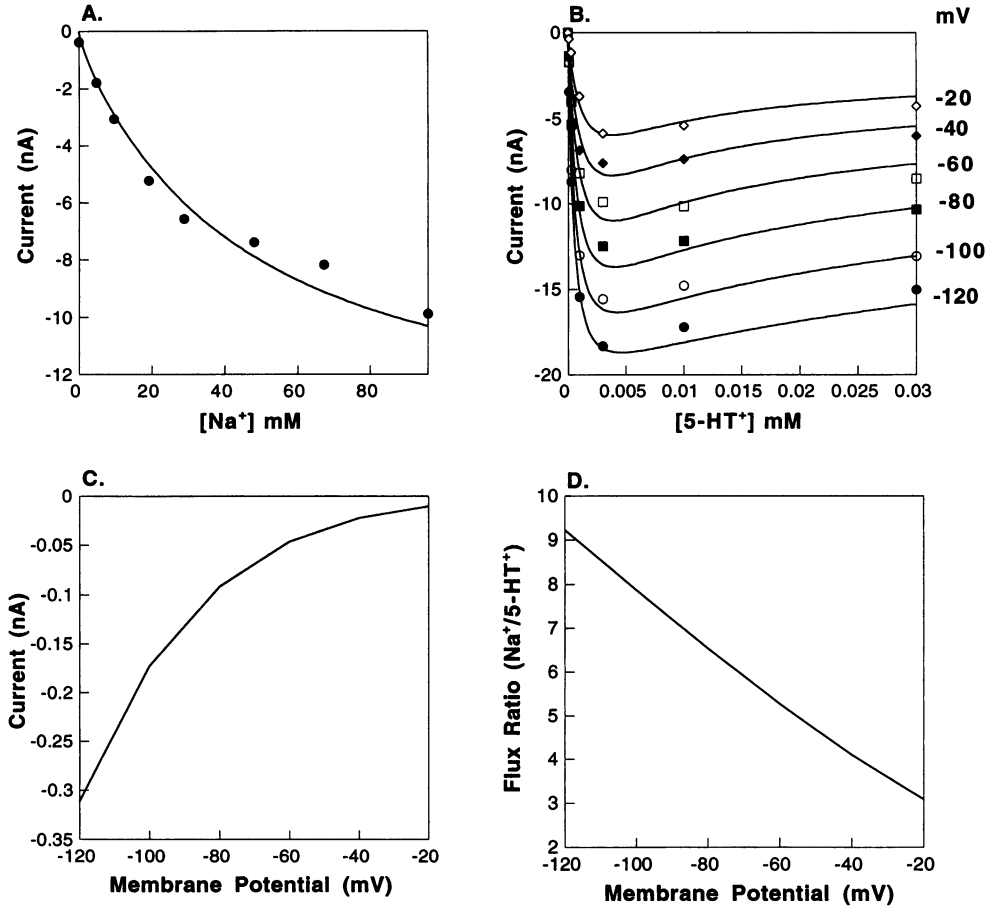

FIGURE 7 Simulated versus experimental 5-HTT steady-state properties. (*A*) Steady-state current as a function of [5-HT$^+$]. Experimental data were taken at [Na$^+$] = 96 mM, with the membrane potential varying from −120 to −20 mV (Mager et al., 1994). (*B*) Steady-state current as a function of [Na$^+$]. Data were taken at [5-HT$^+$] = 3 μM, with membrane potential set to −60 mV (Mager et al., 1994). (*C*) Simulated leakage current at zero 5-HT, under the same experimental conditions as in *A*. (*D*) Flux ratio of Na$^+$ to 5-HT$^+$ simulated at [Na$^+$] = 96 mM, [5-HT$^+$] = 1 μM, versus membrane voltage.

The experimentally determined permeation properties of 5-HTT include its steady-state currents as a function of Na$^+$ and 5-HT$^+$, leakage currents (Na$^+$ flux in the absence of 5-HT$^+$), and variable stoichiometry (5–12 Na$^+$ transported per 5-HT$^+$) (Mager et al., 1994). The phenomena of leakage currents and variable stoichiometry are not expected from the alternating access model. The simulation reproduced the above experimental results under one set of model parameters. The simulated 5-HTT steady-state current showed a nonsigmoidal dependence on [Na$^+$] (Fig. 7 *A*) and a biphasic dependence on [5-HT$^+$] (Fig. 7 *B*). Leakage currents on the order of 1 nA were observed in the absence of external 5-HT$^+$ (Fig. 7 *C*). An important feature of 5-HT transport is its variable stoichiometry (voltage-dependent flux ratio of Na$^+$/5-HT$^+$). This is simulated in Fig. 7 *D*.

We comment here on several critical parameters that underlie two unique permeation properties of the 5-HT transporter: the nonsigmoidal dependence on [Na$^+$] and the biphasic dependence on [5-HT$^+$]. The nonsigmoidal dependence can be made sigmoidal by increasing the population of transporter configurations 5, 6, 7 (occupied by two Na$^+$) relative to 2, 3, 4 (occupied by one Na$^+$). The biphasic dependence can be abolished either a) by increasing the intrinsic hopping frequency ratio between Na$^+$ and 5-HT$^+$ or b) by increasing the positive coupling between 5-HT$^+$ and its modulators. This implies that the slower movement of 5-HT$^+$ can block the movement of Na$^+$, thereby causing decreasing current at higher [5-HT$^+$].

Simulation of SGLT1 function

SGLT1 is a Na$^+$/glucose cotransporter that shares a postulated membrane topology and functional properties with GAT1 (Wright, 1993). Na$^+$ and sugar (the nonmetabolizable derivative α-methyl-D-glucose is typically used in physiological studies) appear to be the only substrates; thus the number and charge of its substrates equal those for the simplified model of GAT1 discussed above. SGLT1 has been modeled previously as a carrier (Parent et al., 1992b). Our simulations approximated the *I-V* curves (Fig. 8, *A* and *B*) and the experimental substrate flux ratio (Fig. 8 *C*) under one set of model parameters. Table 2 reveals that several of the kinetic parameters for SGLT1 are greater than those for GAT1, so that SGLT1 has an overall higher turnover rate.

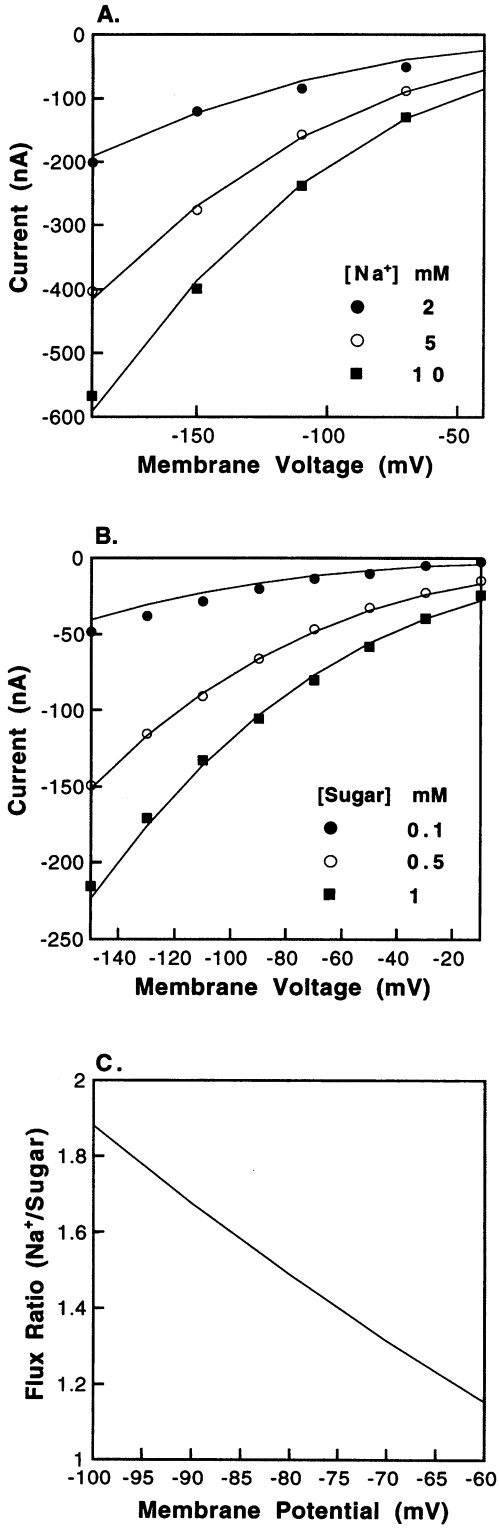

FIGURE 8 Simulated versus experimental SGLT1 steady-state properties. (*A*) Steady-state current as a function of membrane potential. Experimental data were taken at [sugar] = 1 mM, with [Na^+] varying from 2 to 10 mM and as indicated. (*B*) Steady-state current as a function of membrane potential. Data were taken at [Na^+] = 10 mM, with [sugar] varying from 0.1 to 1 mM and as indicated. Assumed number of transporters in the membrane for *A* is roughly twice that for *B*. (*C*) Flux ratio of Na^+ to [sugar] simulated at [Na^+] = 10 mM, [sugar] = 6 mM, as a function of voltage from −100 to −60 mV.

There are also differences in the electrical positions of the binding sites between these two transporters, accounting for the different voltage sensitivities of transport.

DISCUSSION

Our simulations show that it is possible to account for the major features of ion-coupled transport without invoking explicit conformational changes that control the compartmentalization of substrates. The present multi-substrate single-file transport model differs from the usual alternating access models, which suggest that the transporter possesses a "gate" at both ends of the lumen, that the gates are alternately exposed to one side of the membrane, and that the gating is controlled by substrate binding at appropriate sites and with appropriate stoichiometry. In the multi-substrate single-file transport framework, the only structural assumption is the protein's capability to provide a linear lumen and to mediate substrate-substrate interactions. This assumption seems plausible in light of present knowledge about permeation through ion channels.

Ion-coupled transporters show a wide range of permeation properties, including leakage currents, variable stoichiometry, substrate flux coupling, and voltage-dependent transients. Alternating-access models account for only some of these properties. Tight substrate flux coupling and voltage-dependent charge movements naturally result from these models, whereas variable stoichiometry and leakage currents are inherently hard to explain with these models. In contrast, the present scheme covers a broad spectrum of permeation properties. It can be applied to GAT1, which shows leakage currents, tight substrate flux coupling, and voltage-dependent gating currents. The model can also be used to interpret the variable stoichiometry of the 5-HT transporter. The flexibility of the model can be largely attributed to the minimal assumptions made about transporter structures. One of our colleagues remarked that our model resembles a diffusion pump.

Transport cycles

In an alternating-access model (see, for instance, Rudnick and Clark, 1993), there is a definite series of transitions among steps, looping back to a starting state after a complete set of substrates has been transported; and this series constitutes the transport cycle. In the multi-substrate single-file transport model, there are many more possible states than in other models; which are the major steps in the transport cycle? To address this question, we trace out major transport cycles in Fig. 2 as follows. We start from the empty transporter (configuration 1) and choose the transition with the highest net flux. If the two greatest net fluxes differ by less than 5%, we choose both. These steps are repeated until closed loops are formed. Fig. 9 *A* shows the subset of states and transitions from Fig. 2 that are included in the two major transport cycles for GAT1, under the same experimental conditions as in Fig. 4 *D*. The two transport

TABLE 2 Optimized parameter values for GAT1, 5-HT, and SGLT1

Parameter	Physical meaning	Units	GAT1	5-HT transporter	SGLT1
k_1	Forward binding constant (Na^+)	$M^{-1}s^{-1}$	170.	56.3	6.1×10^5
k_2	Forward binding constant (organic substrate)	$M^{-1}s^{-1}$	6.45×10^5	35,100	3.1×10^5
h_1	Intrinsic hopping frequency (Na^+)	s^{-1}	1.02	3.59	340
h_2	Intrinsic hopping frequency (organic substrate)	s^{-1}	12.6	1.00	1055
d_1	Electrical location of binding sites ($0 < d < 1$)		0.5	0.509	0.164
d_2			0.692	0.701	0.674
d_3			0.8	0.901	0.894
A_{10}	Attractive interaction between Na^+ and an empty site		0.133	8.62×10^{-3}	6.42×10^{-7}
A_{20}	Attractive interaction between organic substrate and an empty site		0.05	6.85	1.23
A_{11}	Attractive interaction between Na^+ and Na^+		9.83	9.79	4.04
A_{12}	Attractive interaction between Na^+ and organic substrate		40001	2.73	8.61
A_{22}	Attractive interaction between organic substrate and organic substrate		40.5	0.0526	0.297
R_{10}	Repulsive interaction between Na^+ and an empty site		9.74	1.04	0.506
R_{20}	Repulsive interaction between organic substrate and an empty site		60.5	3.35×10^{-3}	8.21
R_{11}	Repulsive interaction between Na^+ and Na^+		0.257	3.42	9.70
R_{12}	Repulsive interaction between Na^+ and organic substrate		10001	4.05	2.07
R_{22}	Repulsive interaction between organic substrate and organic substrate		701	8.38	8.73
ΔG_{10}	Repulsive interaction between Na^+ and an empty site		2.54	2.84	8.04
ΔG_{20}	Repulsive interaction between organic substrate and an empty site		4.20	−4.51	1.12
ΔG_{11}	Repulsive interaction between Na^+ and Na^+		−2.16	−0.62	0.52
ΔG_{12}	Repulsive interaction between Na^+ and organic substrate		−0.82	0.23	−0.84
ΔG_{22}	Repulsive interaction between organic substrate and organic substrate		1.69	3.00	2.00

For GAT1, 5-HTT, and SGLT1, five, eight, and two sets of parameters (respectively) yielded nearly equal cost function values for the steady-state data. For GAT1, the parameters given are those that also simulated the transient data (see Fig. 5). For the 5-HT transporter and SGLT1, parameters with the lowest cost function values are presented. Substrate 1 = Na^+ in all cases. For GAT1, 5-HTT, and SGLT1, substrate 2 = GABA, 5-HT^+, and sugar, respectively.

cycles operate simultaneously; one releases a Na^+, and the other releases both a Na^+ and a GABA. Together, they provide an explanation for the observed substrate flux ratio ($1 < Na^+/GABA < 2$).

To understand the origin of "variable stoichiometry," a similar transport cycle analysis is applied to the 5-HT transporter (Fig. 9 *B*). The transport cycle couples one 5-HT^+ release to a loop of Na^+ releases. This loop may be responsible for the observed variable stoichiometry, because various numbers of Na^+ molecules can be released per 5-HT^+ molecule. If this hypothesis is correct, it can further explain the voltage dependence of variable stoichiometry (Fig. 7 *D*). Upon hyperpolarizing, the steady-state population of transporter configurations 5, 6, 7 and the transition frequency from configuration 3 to 5 are both increased, which accelerates the loop and stimulates more Na^+ flux per 5-HT^+ molecule transported.

Computational strategy

Most previous modeling studies have used the King-Altman diagrammatic method to analyze the steady-state distribution of transporters (e.g., Hill, 1977). However, the number of King-Altman patterns increases dramatically as the number of states increases. This constrains the number of practical carrier states. One could in principle automate the King-Altman procedure to analyze more complicated kinetic schemes. However, the time required to list the King-Altman patterns grows as N^{N-1}, where N is the number of carrier states. The present model uses Gauss-Jordan elimination to solve the steady-state distribution. Gauss-Jordan elimination is computationally different from the King-Altman diagrammatic method, but gives the same solution. Because Gauss-Jordan elimination scales as N^3, where N is the number of carrier states, it allows for the consideration of a significantly larger number of states.

Limitations and future directions

The major limitation of our theory in its present form is its inability to deal with the phenomena of antiport, countertransport, exchange, or counterflow, as exemplified by Na^+/Ca^{2+} exchangers, by the glutamate trans-

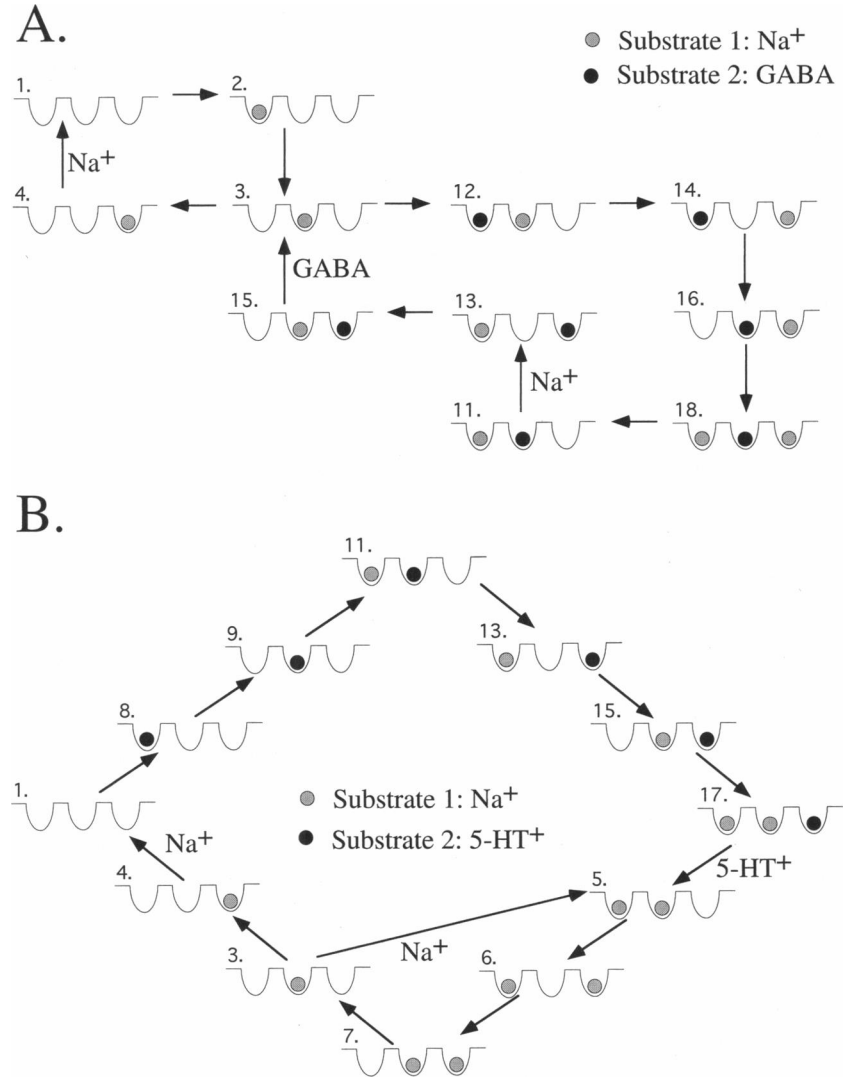

FIGURE 9 Major transport cycles for GAT1 and 5-HTT. (*A*) Major transport cycles for GAT1 traced out by the method described in text. Two transport cycles operate simultaneously. Together, they provide an explanation to the observed substrate flux ratio ($1 < Na^+/GABA < 2$). (*B*) Major transport cycles for 5-HTT. The cycle couples one $5\text{-}HT^+$ release to a loop of Na^+ releases. This loop may be responsible for the observed variable stoichiometry.

porters of the nervous system, by the 5-HT transporter (Rudnick and Clark, 1993), and under some conditions by GABA transporters (Mabjeesh and Kanner, 1989). Fig. 6 shows that our model does simulate a small (20–50%) increased influx through GAT1 as internal [GABA] is increased; but we have not systematically studied this effect. We suspect that models with alcoves or Y-shaped lumens would be required to account for robust antiport (Eisenberg, 1994).

The model is also uninformative about other aspects of transporter function. It neglects the frank channel activity, with conductances on the order of picosiemens, that has recently been observed with GAT1 (Cammack and Schwartz, 1995) and with the 5-HT transporter (F. Lin et al., unpublished observations) and inferred from noise studies (see Introduction). Finally, we have not yet considered ATPase transporters.

We do not wish to imply that our model treats the lumen of the transporter as a featureless series of chemically inert pockets. We suspect that movements of the side chains lining the lumen could provide the attractive and repulsive interactions (quantified by A_{ij} and R_{ij}) that we postulate. We emphasize, however, that we view these motions as local, probably restricted to <0.5 nm from the bound substrates in question, as opposed to the global changes in compartmentalization that characterize alternating-access models. Some of the interactions represented by the optimized parameters disagree with intuition; for instance, rule 4 suggests that two neighboring Na^+ ions constitute a relatively stable configuration. Such interactons might be produced by side chains that interpose between two substrates, leading either to charge pairs or to cation-pi interactions between substrates and side chains (Dougherty, 1995).

Structure of ion-coupled transporters

Our theory must remain at the formal level, primarily because we know so little about transporter structure. Although we do know the primary amino acid sequence

for the transporters simulated here, there is no proof for topology diagrams postulated on the basis of the sequence, no information about secondary or tertiary structure, and little data about the residues that actually line the lumen that we postulate. Until such information becomes available, there is little objective reason to choose our model over the alternating-access model and its variants. Although some may prefer the present model because of its simplicity, nature does not seem to prefer simple mechanisms for her macromolecuar machines.

CONCLUSION

The hypothesis of "multi-substrate single-file transport" has been tested and found to account quantitatively for the steady-state data of ion-coupled transporters GAT1, 5-HTT, and SGLT1. In addition, the model predicts the GAT1 transporter's transient responses to voltage and concentration jumps. The model also simulates transport up a concentration gradient, an important feature of ion-coupled transporters. Model analysis such as major transport cycles gives insights about the tight flux coupling of GAT1, leakage currents, and variable stoichiometry of 5-HT transport. Inspection of model parameter values yields a set of microscopic rules that may explain the simulated population distribution of transporter configurations. The success of the model suggests that concepts such as "alternating access" or "gates" are not necessary in interpreting existing experimental results and perhaps can be recast into the present, more general, framework.

We thank Eric Bax, Bassil Dahiyat, Norman Davidson, and Jun Li for suggestions. Scott Fraser suggested the diffusion pump analogy.

This work was supported by grants from the National Institute of Neurological Diseases and Stroke and the National Institute on Drug Abuse. SLM acknowledges support from the Rita Allen Foundation, the David and Lucille Packard Foundation, and the Searle Scholars Program.

REFERENCES

Amara, S. G., and J. L. Arriza. 1993. Neurotransmitter ion-coupled transporters: three distinct gene families. *Curr. Opin. Neurobiol.* 3:337–344.

Andersen, O. S., J. E. N. Silveira, and P. R. Steinmetz. 1985. Intrinsic characteristics of the proton pump in the luminal membrane of a tight urinary epithelium. The relation between transport rate and $\Delta\mu$H. *J. Gen. Physiol.* 86:215–234.

Baldwin, S. A. 1993. Mammalian passive glucose ion-coupled transporters: members of an ubiquitous family of active and passive transport proteins. *Biochim. Biophys. Acta.* 1165:17–49.

Barnett, J. E. G., G. D. Holman, R. A. Chalkley, and K. A. Munday. 1975. Evidence for two asymmetric conformational states in the human erythrocyte sugar-transport system. *Biochem. J.* 145:417–429.

Cammack, J. N., S. V. Rakhilin, and E. A. Schwartz. 1994. A GABA ion-coupled transporter operates asymmetrically and with variable stoichiometry. *Neuron.* 13:1–20.

Cammack, J. N., and E. A. Schwartz. 1993. Ions required for the electrogenic transport of GABA by horizontal cells of the catfish retina. *J. Physiol.* 473:81–102.

Cammack, J. N., and E. A. Schwartz. 1995. Channel behavior in a GABA transporter. *Proc. Natl. Acad. Sci. USA.* In press.

Chen, D. P., and R. S. Eisenberg. 1993. Flux, coupling, and selectivity in ionic channels of one conformation. *Biophys. J.* 65:727–746.

Dani, J. A., and D. G. Levitt. 1990. Diffusion and kinetic approaches to describe permeation in ionic channels. *J. Theor. Biol.* 146:289–301.

DeFelice, L. J., R. Galli, and D. Blakely. 1995. Current fluctuations in norepinephrine transporters. *Biophys. J.* 68:A232.

Dougherty, D. A. 1995. Cation-π interactions in chemistry and biology. *Science.* In press.

Eisenberg, R. S. 1994. Atomic biology, electrostatics, and ionic channels. *In* New Developments and Theoretical Studies of Proteins. Ron Elbor, editor. World Scientific Publishing, Philadelphia. 1–116.

Franciolini, F., and W. Nonner. 1994. A multiion permeation mechanism in neuronal background chloride channels. *J. Gen. Physiol.* 104:725–746.

Frolhich, O. 1988. The "tunneling" mode of biological carrier-mediated transport. *J. Membr. Biol.* 101:189–198.

Gadsby, D. C., R. F. Rakowski, and P. De Weer. 1993. Extracellular access to the Na, K pump: pathway similar to ion channel. *Science.* 260:100–103.

Galli, A., L. DeFelice, B.-J. Duke, K. R. Moore, and R. D. Blakely. 1995. Sodium-dependent norepinephrine-induced currents in norepinephrine-transporter-transfected HEK-293 cells blocked by cocaine and antidepressants. *J. Exp. Biol.* 198:2197–2212.

Guastella, J. H., N. Nelson, H. Nelson, L. Czyzyk, S. Keynan, M. C. Midel, N. Davidson, H. Lester, and B. Kanner. 1990. Cloning and expression of a rat brain GABA ion-coupled transporter. *Science.* 249:1303–1306.

Harvey, W. R., and C. L. Slayman. 1994. Coupling as a way of life. *J. Exp. Biol.* 196 (Transporters):1–4.

Hasegawa, H., W. Skach, O. Baker, M. C., Calayag, V. Lingappa, and A. S. Verkman. 1992. A multifunctional aqueous channel formed by CFTR. *Science.* 258:1477–1479.

Hernandez, J. A., and J. Fischbarg. 1994. Transport properties of single-file pores with two conformational states. *Biophys. J.* 67:996–1006.

Hilgemann, D. W., D. A. Nicoll, and K. D. Philipson. 1991. Charge movement during Na^+ translocation by native and cloned cardiac Na^+/Ca^{2+} exchanger. *Nature.* 352:715–718.

Hill, T. L. 1977. Free Energy Transduction in Biology. Academic Press, New York.

Hille, B. 1992. Ionic Channels of Excitable Membranes. Sinauer Associates, Sunderland, MA.

Ingber, L. 1993. Simulated annealing: practice versus theory. *J. Math. Comput. Modelling.* 18:29–57.

Jardetzky, O. 1966. Simple allosteric model for membrane pumps. *Nature.* 211:969–970.

Kanner, B. I., and S. Schuldiner. 1987. Mechanism of transport and storage of neurotransmitters. *CRC Crit. Rev. Biochem.* 22:1–38.

Keynan, S., and B. I. Kanner. 1988. γ-Aminobutyric acid transport in reconstituted preparations from rat brain: coupled sodium and chloride fluxes. *Biochemistry.* 27:12–17.

Kimmich, G. A., and J. Randles. 1988. Na^+-coupled sugar transport: membrane potential-dependent K_m and K_i for Na^+. *Am. J. Physiol.* 255:C486–C494.

Krupka, R. M. 1989. Role of substrate binding forces in exchange-only transport systems. II. Implications for the mechanism of the anion-exchanger of red cells. *J. Membr. Biol.* 109:159–171.

Krupka, R. M., and R. Deves. 1988. The choline carrier of erythrocytes. Location of the NEM-reactive thiol group in the inner gated channel. *J. Membr. Biol.* 101:43–47.

Lagnado, L., K. Cervetto, and P. A. McNaughton. 1988. Ion transport by the Na-Ca exchanger in isolated rod outer segments. *Proc. Natl. Acad. Sci. USA.* 85:4548–4552.

Lauger, P. 1979. A channel mechanism for electrogenic ion pumps. *Biochim. Biophys. Acta.* 552:143–61.

Lauger, P. 1991. Electrogenic Ion Pumps. Sinauer Associates, Sunderland, MA.

Lester, H. A., S. Mager, M. W. Quick, and J. L. Corey. 1994. Permeation properties of neurotransmitter ion-coupled transporters. *Annu. Rev. Pharmacol. Toxicol.* 34:219–249.

Lowe, A. G., and A. R. Walmsley. 1986. The kinetics of glucose transport in human red blood cells. *Biochim. Biophys. Acta.* 857:146–154.

Mabjeesh, N. J., and B. I. Kanner. 1989. Low-affinity γ-aminobutyric acid transport in rat brain. *Biochemistry.* 28:7694–7699.

Mager, S., C. Min, D. Henry, N. Davidson, C. Chavkin, B. Hoffman, and H. A. Lester. 1994. Conducting states of a mammalian serotonin transporter. *Neuron.* 12:845–859.

Mager, S., J. Naeve, M. Quick, C. Labarca, N. Davidson, and H. A. Lester. 1993. Steady states, charge movements, and rates for a cloned GABA ion-coupled transporter expressed in *Xenopus* oocytes. *Neuron.* 10:177–188.

McQuarrie, D. A. 1976. Statistical Mechanics. Harper & Row, New York.

Nakamoto, R. K., R. Rao, and C. W. Slayman. 1989. Transmembrane segments of the P-type cation-transporting ATPases. A comparative study. *Ann. N.Y. Acad. Sci.* 574:165–179.

Parent, L., S. Supplisson, D. D. F. Loo, and E. M. Wright. 1992a. Electrogenic properties of the cloned Na^+/glucose cotransporter. I. Voltage clamp studies. *J. Membr. Biol.* 125:49–62.

Parent, L., S. Supplisson, D. D. F. Loo, and E. M. Wright. 1992b. Electrogenic properties of the cloned Na^+/glucose cotransporter. II. A transport model under nonrapid equilibrium conditions. *J. Membr. Biol.* 125:63–79.

Picaud, S. A., H. P. Larsson, G. B. Grant, H. Lecar, and F. S. Werblin. 1995. A glutamate gated chloride channel with glutamate transporter-like properties in cone photoreceptors of the tiger salamander. *J. Neurophysiol.* 74:1760–1771.

Press, W. H., S. A. Teukolsky, W. T. Vetterling, and B. P. Flannery. 1992. Numerical Recipes in c. 36–41. Cambridge University Press, Cambridge.

Rakowski, R. F. 1993. Charge movement by the Na/K pump in *Xenopus* oocytes. *J. Gen Physiol.* 101:117–114.

Risso, S., L. DeFelice, and R. D. Blakely. 1995. Sodium-dependent GABA-induced current in GAT1-transfected HeLa cells. *J. Physiol.* In press.

Rudnick, G., and J. Clark. 1993. From synapse to vesicle: the reuptake and storage of biogenic amine neurotransmitters. *Biochim. Biophys. Acta.* 1144:249–263.

Schultz, S. G. 1980. Basic Principles of Membrane Transport. Cambridge. University Press, Cambridge. 33–41, 85, 95, 96.

Schultz, S. G. 1986. Ion-coupled transport of organic solutes across biological membranes. *In* Membrane Physiology. T. E. Andreoli, J. F. Hollfman, D. D. Fanestil, and S. G. Schultz, editors. Plenum Press, New York. 283–294.

Schwartz, E. A., and M. Tachibana. 1990. Electrophysiology of glutamate and sodium co-transport in a glial cell of the salamander retina. *J. Physiol.* 426:32–80.

Stein, W. D. 1986. Transport and Diffusion across Cell Membranes. Academic Press, Orlando, FL. 337–361, 613–616.

Umbach, J. A., M. J. Coady, and E. M. Wright. 1990. Intestinal Na^+/glucose cotransporter expressed in *Xenopus* oocytes is electrogenic. *Biophys. J.* 57:1217–1224.

Wadiche, J. I., S. G. Amara, and M. P. Kavanaugh. 1995b. Ion fluxes associated with excitatory amino acid transport. *Neuron.* 15: 721–728.

Wadiche, J. I., J. L. Arriza, S. G. Amara, and M. P. Kavanaugh. 1995a. Kinetics of a human glutamate transporter. *Neuron.* 14:1019–1027.

Walmsley, A. R. 1988. The dynamics of the glucose ion-coupled transporter. *Trends Biochem. Sci.* 13:226–231.

Wang, J. S., J. M. Tang, and R. S. Eisenberg. 1992. A calcium conducting channel akin to a calcium pump. *J. Membr. Biol.* 130:163–181.

Wright, E. M. 1993. The intestinal Na^+/glucose ion-coupled cotransporter. *Annu. Rev. Physiol.* 55:575–89.